Chapter 4
Imaging of Renal Tumors

Steven P. Rowe, Yafu Yin, and Michael A. Gorin

Introduction

The incidence of clinically localized renal tumors has gradually increased in recent decades, paralleling the growing use of cross-sectional imaging across the field of medicine [1, 2]. The most common primary tumor of the kidney is renal cell carcinoma (RCC), representing up to 90% of all renal masses [3]. The International Society of Urologic Pathology now recognizes a number of histologic subtypes of RCC, each with their own molecular underpinnings and metastatic potential [4]. The most common of these are the clear cell (~75%), papillary (~15%), and chromophobe (~5%) RCC subtypes. In general, clear cell RCC and type II papillary RCC are categorized as aggressive, whereas type I papillary RCC and chromophobe RCC are thought to behave in a more indolent manner. Less common RCC subtypes include clear cell papillary RCC, translocation-associated RCC, medullary RCC, and collecting duct RCC. Benign renal tumor histologies include oncocytomas, angiomyolipomas (AMLs), and mixed epithelial stromal tumors (MESTs).

Anatomical imaging with X-ray computed tomography (CT), magnetic resonance imaging (MRI), and ultrasound (US) plays an important role in the detection and characterization of renal masses. However, these conventional imaging

S. P. Rowe (✉) · M. A. Gorin
The Russell H. Morgan Department of Radiology and Radiologic Science, Johns Hopkins University School of Medicine, Baltimore, MD, USA

The James Buchanan Brady Urological Institute and Department of Urology, Johns Hopkins University School of Medicine, Baltimore, MD, USA
e-mail: srowe8@jhmi.edu

Y. Yin
The Russell H. Morgan Department of Radiology and Radiologic Science, Johns Hopkins University School of Medicine, Baltimore, MD, USA

The Department of Nuclear Medicine, The First Hospital of China Medical University, Shenyang, China

M. A. Gorin, M. E. Allaf (eds.), *Diagnosis and Surgical Management of Renal Tumors*, https://doi.org/10.1007/978-3-319-92309-3_4

techniques are often unable to provide specific information regarding the histology of a renal mass. This information is of clinical importance, as a significant portion of renal tumors will be a benign or indolent histology not requiring surgical intervention [5]. To aid in minimizing the overtreatment of clinically insignificant renal tumors, investigational techniques such as molecular imaging are being evaluated for their ability to noninvasively determine the histology of renal tumors [6, 7]. In this chapter, we review the role of anatomical and molecular imaging in the evaluation of renal masses.

Imaging of Renal Tumors

X-Ray Computed Tomography

The most commonly used modality for renal mass characterization is multiphase CT. CT is widely available and provides for high intrinsic spatial resolution. Initial evaluation of a renal mass with CT should be carried out in four phases with a non-contrast acquisition followed by post-contrast imaging in the arterial, venous, and delayed phases. This study is commonly referred to as a renal protocol CT. Of note, at least one of the post-contrast CT acquisitions can be extended beyond the kidney to cover the entire chest, abdomen, and pelvis in order to evaluate for the presence of metastatic disease.

When performing a renal protocol CT, a non-contrast phase is acquired just prior to contrast administration. This allows for differentiation between hyperdense renal cysts and true enhancing masses by providing a baseline attenuation that can be compared to subsequent contrast phases. More specifically, a cyst will remain the same density throughout all phases of the study (±10 Hounsfield units), whereas a solid mass will show increased attenuation following intravenous contrast administration. Next, arterial or corticomedullary phase images are acquired 25–30 s following the administration of intravenous contrast. Many common renal tumors, most notably clear cell RCC and oncocytomas, are highly conspicuous at this imaging time point owing to brisk arterial enhancement (Fig. 4.1) [8]. It should be noted, however, that the high level of enhancement of the cortex can obscure small and peripherally located masses.

A venous or nephrographic phase is next acquired. This is performed at approximately 80–90 s after contrast administration. This phase has particular utility in the identification of small renal masses and can aid in identifying tumor invasion of the ipsilateral main renal vein and/or inferior vena cava (Fig. 4.2) [9]. Finally, a delayed or urographic phase is performed 5–8 min following contrast administration in order to evaluate the renal collecting system, which can be useful for detecting coexisting pathologies such as transitional cell carcinoma.

Renal protocol CT can also provide other potentially important information regarding a renal mass. For example, any of the CT phases can be utilized to examine for the presence of extension of tumor beyond the kidney capsule, albeit with lim-

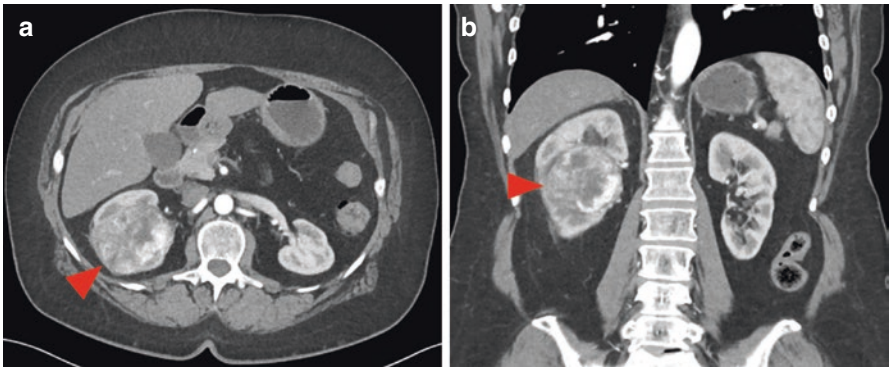

Fig. 4.1 CT images of a clinically localized clear cell RCC. (**a**) Axial and (**b**) coronal, arterial phase images. Note the brisk arterial enhancement in this tumor (red arrowheads) particularly along the inferomedial aspects of the lesion. This enhancement pattern is typical for clear cell RCC

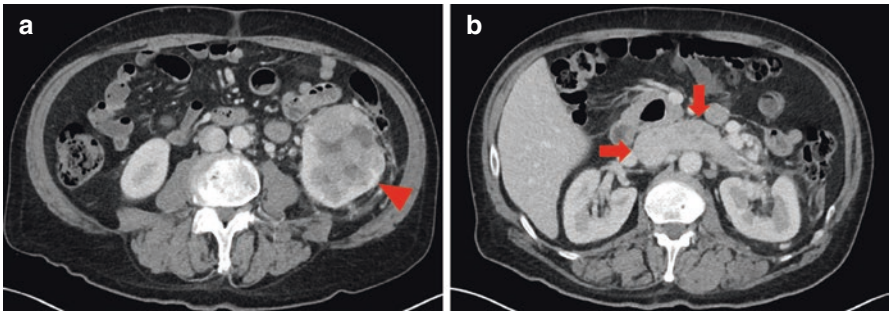

Fig. 4.2 CT images of a clear cell RCC with venous invasion. (**a**) Axial, venous phase image shows a large heterogeneously enhancing left-sided renal mass (red arrowhead). (**b**) In a more superior axial, venous phase CT image, the left renal vein and inferior vena cava are enlarged with internal heterogeneous enhancement (red arrows), compatible with venous invasion of the tumor. Following imaging the mass was surgically resected and was found to be clear cell RCC

ited sensitivity [10]. Additionally, this study can be useful for determining the histology of selected renal masses. Perhaps the best example of this is for AMLs, as the vast majority of these lesions contain macroscopic fat that is visualized as areas of negative Hounsfield units on CT (Fig. 4.3). Aside from AMLs, the ability of CT to characterize the histology of a given renal mass is limited, although some general trends are worth noting. For example, papillary RCC generally demonstrates a low and relatively homogeneous level of enhancement in comparison to clear cell RCC and oncocytomas, with chromophobe RCC most often having an intermediate enhancement level [8].

Cystic renal lesions are well-characterized by CT and are deserving of detailed discussion. The Bosniak classification of renal cysts has been in common use since its introduction in 1986 [11]. With this classification system, cystic lesions are divided into five categories (I, II, IIF, III, and IV) with an

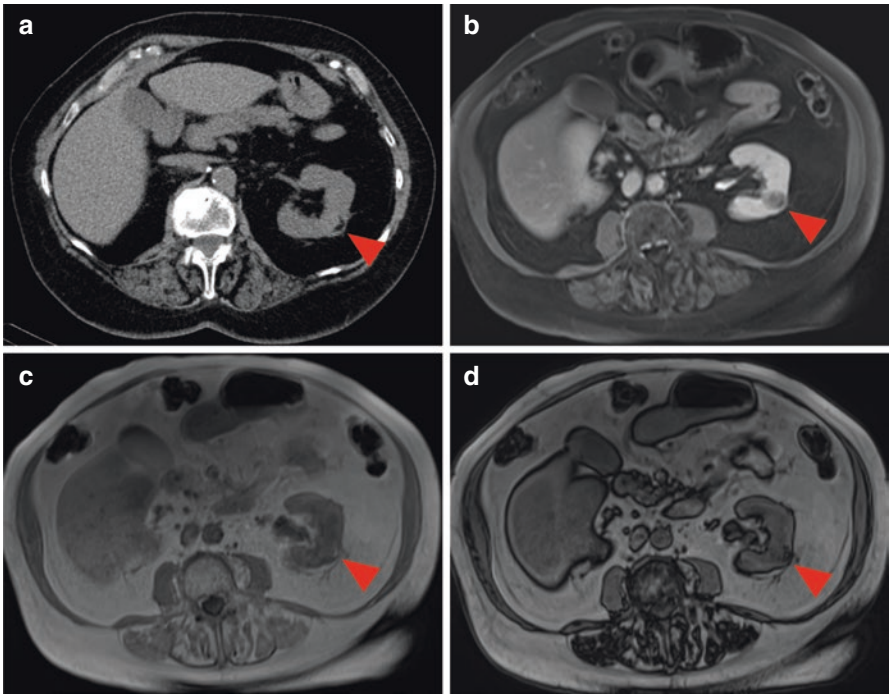

Fig. 4.3 CT and MRI images of a renal AML. (**a**) Axial, non-contrast CT image of a patient with a left-sided renal mass containing macroscopic fat (red arrowhead). Note that the attenuation of the fat in the mass is identical to the perinephric fat surrounding the kidney. (**b**) Axial, T1, fat-saturation, post-contrast MR image in the same patient delineates the borders of this relatively hypoenhancing tumor and also demonstrates the presence of macroscopic fat. Just as on CT, the crescentic area of fat within the AML appears identical to the perinephric fat. (**c**) Axial, in-phase and (**d**) axial, out-of-phase MR images show the area of macroscopic fat in the AML as bright/high signal on the in-phase image (**c**), whereas the periphery of the macroscopic fat becomes dark/low signal on the out-of-phase image. This finding is known as the India ink artifact

increasing risk of underlying malignancy in the higher numerical categories. Bosniak I lesions are simple epithelial cysts which are a common incidental finding on CT. These lesions are not true tumors of the kidney, as they lack any solid component and are universally benign. Bosniak I cysts are simple fluid attenuation on CT (generally taken to be ≤20 Hounsfield units) and do not have any visible septa or calcifications. The Bosniak II classification includes benign cystic lesions that are not pure simple epithelial cysts. These lesions can contain a few thin septations (without visible or measurable enhancement), minimal associated calcifications, or measure greater than simple fluid attenuation [12]. Both Bosniak I and II cysts should be well-circumscribed with easily definable boundaries with the adjacent normal renal parenchyma. Lesions in either of these categories do not require any specific follow-up or intervention except for in symptomatic individuals.

Bosniak IIF cysts are often the most difficult to accurately categorize as many different features can place a cystic lesion in this category (Fig. 4.4). Characteristics of Bosniak IIF lesions include the presence of several thin septa, apparent visual but not measurable enhancement of a cyst wall or septum, non-enhancing smooth or nodular thickening of a wall or septum, and more-than-minimal associated calcifications. The risk of malignancy with these lesions is thought to be on the order of 5%; thus follow-up but not immediate treatment is required [13].

Bosniak III (Fig. 4.5) and IV (Fig. 4.6) cystic lesions harbor a high likelihood of malignancy and should be managed with surgical resection. Bosniak III cysts demonstrate measurably enhancing walls or septa, which can be smooth or irregular, and approximately 50% of these lesions are malignant [14]. Bosniak IV lesions contain

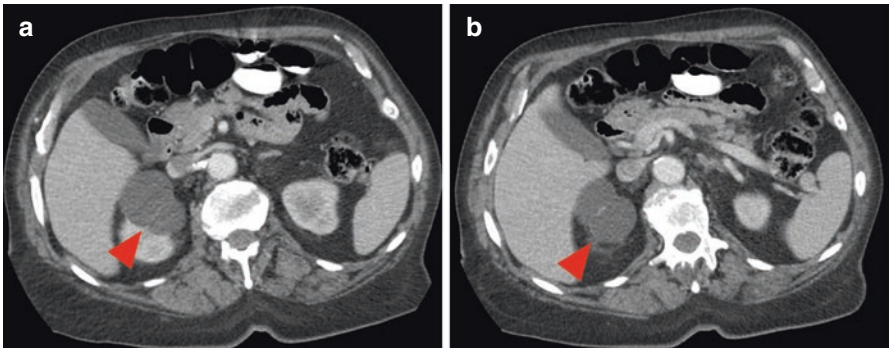

Fig. 4.4 CT images of a Bosniak IIF renal cyst. (**a**) Axial, venous phase image of a minimally complex right-sided renal cystic lesion. A thin septation (red arrowhead) is apparent within the cystic lesion. (**b**) On a more superior axial, venous phase image, a smooth thickening of the septation is apparent with visual enhancement, although the septation is too thin to reliably measure this enhancement (red arrowhead)

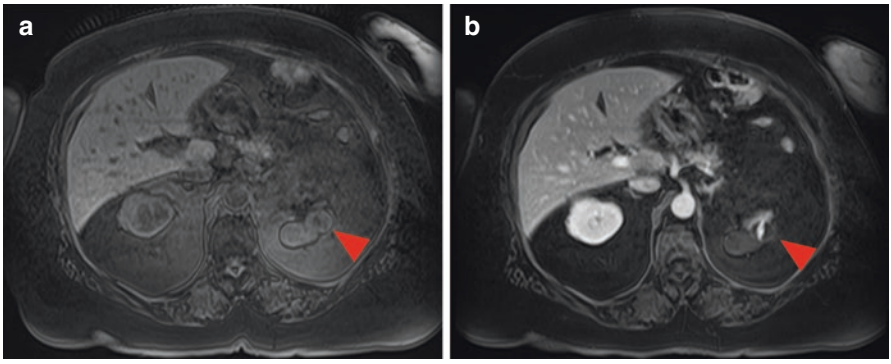

Fig. 4.5 MRI images of a multi-lobulated Bosniak III cyst. (**a**) Axial, T1, fat-saturation, non-contrast image and (**b**) axial, T1, fat-saturation, post-contrast MR image. Note the thick, avidly enhancing septum in the lesion (red arrowheads)

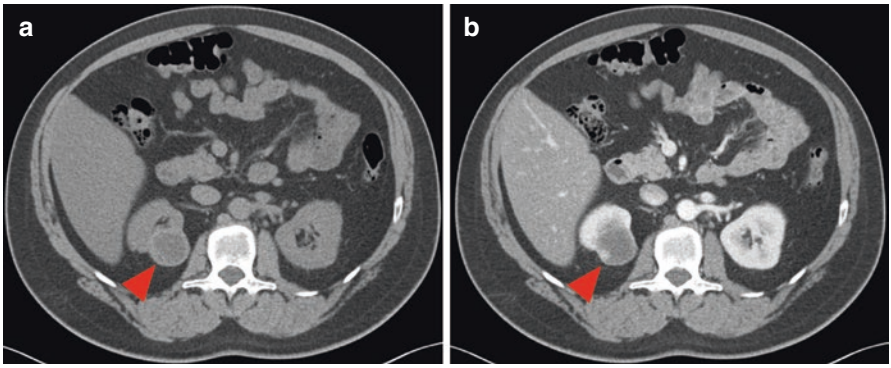

Fig. 4.6 CT images of a Bosniak IV renal cyst. (**a**) Axial, non-contrast image of a predominantly low-density right renal lesion that does visually appear to be a simple cyst (red arrowhead). (**b**) Axial, venous phase CT demonstrates that much of the lesion does not enhance; however a nodular, enhancing component is present within the wall of this cystic lesion (red arrowhead)

definitive, enhancing solid components and are true renal tumors. These lesions are most often cystic RCCs and should be treated as malignant, although some other rare renal neoplasms may present as Bosniak IV cysts [15].

Magnetic Resonance Imaging

MRI of renal tumors parallels the evaluation that takes place with CT, with some important differences imposed by the longer scan acquisition time and other technical parameters. The American College of Radiology considers multiphase CT to be the best method by which to evaluate an indeterminate renal mass, although multiphase MRI is also considered appropriate [16]. MRI offers advantages in soft tissue characterization and functional imaging. Additionally, MRI lacks ionizing radiation, which may be an important consideration in younger patients with renal malignancies requiring multiple examinations for surveillance. Renal protocol MRI provides much of the same information as CT such as anatomic delineation of a renal tumor and its enhancement characteristics. Generally, renal protocol MRI should be carried out on a closed MRI operating at 1.5 T or 3.0 T field strength. Typically, the pulse sequences included in a renal protocol MRI include T1-weighted pre-contrast images (with both in-phase and opposed-phase acquisitions allowing for identification of fat and water within a single voxel), T2-weighted images, and post-contrast T1 imaging in multiple phases as is performed for CT [17]. The renal collecting system is best evaluated on delayed-phase post-contrast imaging with fat saturation. Modern renal protocol MRI often also includes diffusion-weighted imaging (DWI), which measures restriction in the motion of water and is often regarded as a surrogate for cellularity. DWI is interpreted in conjunction with an apparent diffusion coefficient (ADC) map that confirms that high signal on DWI is

true diffusion restriction and is not a manifestation of high T2 signal in the tumor. True diffusion restriction will demonstrate low signal on an ADC map, whereas a falsely high DWI signal as the result of associated high T2 signal will also have high signal on an ADC map.

The determination of renal mass histology is somewhat limited with MRI, although there are some advantages relative to CT. As with CT, the most definitive diagnosis can often be made with AMLs, again through the identification of macroscopic fat within the tumor which will have high signal intensity on both T1- and T2-weighted images with signal drop-out with chemical shift fat saturation and India ink artifact at fat-soft tissue interfaces with opposed-phase imaging (Fig. 4.3). Interestingly, the presence of intracellular or microscopic fat can cause a more generalized loss of signal on opposed-phase imaging than what is seen with the India ink artifact, and this non-specific finding can be present with either clear cell RCC or AMLs [18].

As with CT, the general rule applies with contrast-enhanced MRI that clear cell RCC and oncocytomas are the most hyperenhancing renal masses, with papillary RCC being overall hypoenhancing and chromophobe RCC demonstrating intermediate levels of enhancement. However, the improved soft tissue characterization of MRI relative to CT and the inclusion of the functional information available from DWI may allow for relative confidence in the differentiation of some tumor types [19]. For example, although both clear cell RCC and AMLs can demonstrate signal drop on opposed-phase imaging, this finding in a solid renal mass that is homogeneous and demonstrates low signal on T2-weighted imaging is diagnostic of an AML [20]. DWI has shown promise in differentiating aggressive from benign tumors, with significantly lower ADC values present in RCCs in comparison to oncocytomas [21]. Among RCC subtypes, papillary RCC often demonstrates very low ADC values compatible with restricted diffusion, although other subtypes with high nucleolar grades can also be low signal on ADC maps [22].

Cystic renal lesions on MRI are also well-characterized, and the previously described Bosniak categories can still be used [23]. Most cystic renal lesions will have the same Bosniak classification whether imaged with CT or MRI, although MRI does appear to have a higher sensitivity for septa, wall and septal thickening, and subtle enhancement of the wall and septa. As such, some cystic lesions will have higher Bosniak classifications on MRI, which can affect the preferred management strategy [23]. A pure, benign, Bosniak I epithelial cyst should appear on MRI as a very T2 bright and T1 dark lesion without any evidence of contrast enhancement, following the signal characteristics of simple fluid. Calcifications in Bosniak II–IV cysts will show up as areas of low T1 and T2 signal. Any enhancing features in Bosniak II–IV cysts are evaluated on pre- and post-contrast T1 images and will show increased signal on the post-contrast acquisition (Fig. 4.5).

Imaging of the chest is often difficult to perform with MRI due to respiratory and cardiac motion. Although many pulse sequences can now acquire slices during single breath-holds, slice selection can limit evaluation for subtle findings such as small pulmonary nodules. As a result, staging of RCC is often performed with a renal protocol MRI of the abdomen and pelvis along with dedicated chest imaging (preferably CT).

Ultrasound

US evaluation of renal masses is somewhat limited in comparison to CT and MRI, although the emergence of US-compatible intravenous contrast agents may result in evolving practice patterns in coming years. US lacks ionizing radiation and nephrotoxic contrast; however, US can be limited by poor visualization of the kidneys in patients that have a large body habitus. Additionally, this imaging modality is highly operator dependent, a limitation that is not present with CT and MRI. Furthermore, the sensitivity of US for renal masses is lower than other cross-sectional modalities [24]. However, the lack of ionizing radiation of US makes it particularly well suited to following known renal masses for growth. For example, US is used heavily for follow-up in the Delayed Intervention and Surveillance for Small Renal Masses (DISSRM) Registry that aims to decrease overtreatment of small renal masses [25].

As with CT and MRI, the underlying histology of a solid renal mass is often unable to be characterized on US. Solid renal masses can demonstrate a variety of echoic properties, with RCCs potentially being hypoechoic, isoechoic, or hyperechoic relative to the background renal parenchyma. Classically, the macroscopic fat in AMLs causes them to be hyperechoic, but this finding can be subtle and is not nearly as definitive as the identification of fat on CT or MRI.

US has excellent discriminatory ability for solid versus cystic masses, particularly when a relatively hypodense lesion is identified on CT that is not a definitive hyperdense cyst [26]. Additionally, US has a high sensitivity for septa, debris within cystic lesions, and calcifications. Other than definitive Bosniak I simple epithelial cysts, which appear completely anechoic on US and demonstrate increased through-transmission, other cystic lesions must be graded with renal protocol CT or MRI.

An exciting development in the field of US imaging has been the introduction of intravenous contrast agents. Although the use of US contrast for renal mass imaging is off-label in the United States, early data suggest that contrast agents provide useful information in the characterization of renal tumors [27, 28]. The imaging mechanism of intravenous microbubbles involves the reflection of sonographic signal off of many echogenic surfaces, thus increasing the signal of vascularized tissues. Contrast-enhanced US has shown promise in the characterization of cystic renal lesions [27] and may have improved sensitivity for subtle blood flow within solid renal tumors in comparison to CT [28]. The ultimate utility of contrast-enhanced US in renal tumor imaging does, however, require further exploration.

Molecular Imaging of Renal Tumors

General Background

Although the anatomic information available from conventional imaging is invaluable in the work-up of patients with renal tumors, in most circumstances a histologic characterization of an enhancing renal mass is not readily feasible with these

modalities, as has been noted above. In particular, distinguishing hyperenhancing clear cell RCC from similarly hyperenhancing oncocytomas is particularly difficult. This is distinctly problematic given that these represent the most common malignant and benign renal mass types, respectively. Investigational work has been done to derive additional information from available conventional imaging data, with particularly promising recent work demonstrating that CT texture analysis can somewhat successfully differentiate among different renal tumor histologies, including clear cell RCC and oncocytomas [29]. These methods, however, remain investigational, and larger volumes of data with advanced machine learning/artificial intelligence algorithms are needed in order to utilize standard CT, MRI, and US datasets to adequately classify renal tumors.

The limitations of characterizing renal tumors with CT, MRI, and US have contributed to an interest in developing molecular imaging approaches to better distinguish benign and indolent renal masses from those that are likely to behave in an aggressive manner. The Society of Nuclear Medicine and Molecular Imaging broadly defines the field of molecular imaging as "a type of medical imaging that provides detailed pictures of what is happening inside the body at the molecular and cellular level [30]." Thus, molecular imaging is able to provide functional information about a tumor's underlying biology that is not available from anatomical cross-sectional imaging.

The two most common modalities employed in molecular imaging are positron emission tomography (PET) and single-photon emission computed tomography (SPECT). Fundamentally, PET makes use of positron-emitting radionuclides (including ^{18}F, ^{11}C, ^{68}Ga, ^{124}I, and ^{89}Zr) that are covalently or non-covalently bonded or conjugated to molecules that allow for localization of the radionuclide to a cellular or molecular process of interest. The decay of such radionuclides produces a positron that interacts with surrounding matter, comes to rest, and then annihilates with a nearby electron. This annihilation process produces two 511-keV photons that are given off in opposite directions and are detected at nearly exactly the same time at opposite points around a ring of detectors that surrounds the patient. This process is often referred to as "coincidence detection." The sophisticated electronics of the PET scanner are able to localize these coincidence detection events and record a line of response connecting the two detectors triggered coincidentally. Because the original positron decay event must have occurred along that line or response, the coincidence detection encodes spatial information on where the positron-emitting decay event occurred. Through the collection of many such coincidence events, the system is able to reconstruct images that reflect the distribution of the radiotracer within the patient's body.

SPECT makes use of a fundamentally different process than PET. SPECT relies on single-photon-emitting radionuclides (including ^{99m}Tc, ^{111}In, and ^{123}I), and the coincidence detection that underlies PET is not possible with these radioisotopes. Single-photon emission is an omnidirectional process, with emission of the photons from the radiotracer occurring in such a way that any direction of photon emission is equally likely as any other direction. As such, the imaging process places a collimator between the patient and the detector. A collimator allows only those photons that travel through its holes, which are positioned perpendicular to the patient, to

reach the detector thereby excluding photons that arrive at an angle to the collimator holes, thus imparting spatial information to the created image. A SPECT detector and its associated collimator are slowly rotated around the patient in either a stepwise or continuous manner so that complete volumetric data can be acquired.

The data acquired from these imaging methods are usually reconstructed in a tomographic manner and then combined with anatomic information from CT or less commonly MRI. As such, most modern molecular imaging is actually a combination of molecular and anatomic information.

Radiotracers and Their Targets

The most commonly used molecular imaging agent is the PET radiotracer and glucose analog 2-deoxy-2-[^{18}F]fluoro-D-glucose (^{18}F-FDG). ^{18}F-FDG is a profoundly important radiotracer that has revolutionized the imaging of many malignancies. This imaging agent, however, has not shown an ability to reliably identify or characterize renal tumors [31]. As such, other radiotracers have been investigated for these purposes.

The best studied target for renal mass molecular imaging is carbonic anhydrase IX (CAIX), a cell surface enzyme with a role in maintaining extracellular pH [32]. While in many nonrenal malignancies, CAIX expression is inducible and related to the low oxygen tension of hypoxia, the vast majority of clear cell RCCs constitutively overexpress CAIX as a result of loss of the von Hippel-Lindau tumor suppressor gene [33, 34]. Further enhancing the appeal of CAIX as a target is that it is not found to any measurable extent in normal renal parenchyma or on renal masses other than the clear cell subtype [35–37]. An ^{124}I-labeled monoclonal antibody against CAIX (^{124}I-girentuximab) has proven particularly promising. A pilot study of 26 patients with renal tumors who underwent ^{124}I-girentuximab PET/CT imaging prior to surgical resection found a sensitivity of 94% for the detection of clear cell RCC with no false-positive results [38]. A larger multicenter trial with 195 patients was also promising with a reported sensitivity of 86.2% and specificity of 85.9% for the identification of clear cell RCC [39]. Overall, ^{124}I-girentuximab PET/CT was found to be significantly more sensitive and specific than conventional imaging with contrast-enhanced CT. Given these promising results, other CAIX-targeting agents, including small molecule radiotracers, are also being investigated [40, 41].

^{11}C-acetate, a radiolabeled cholesterol and fatty acid precursor, has also been studied in the context of characterizing otherwise indeterminate renal masses. Imaging with this radiotracer has demonstrated an overall higher sensitivity for detecting RCCs in comparison to ^{18}F-FDG. Additionally, this radiotracer may have a role in the identification of fat-poor AMLs, which have been shown to take up significant amounts of ^{11}C-acetate [42].

Recently, there has been an interest in applying the widely available and inexpensive single-photon-emitting radiotracer ^{99m}Tc-sestamibi for the characterization of anatomically indeterminate renal tumors (Fig. 4.7). ^{99m}Tc-sestamibi is a lipophilic

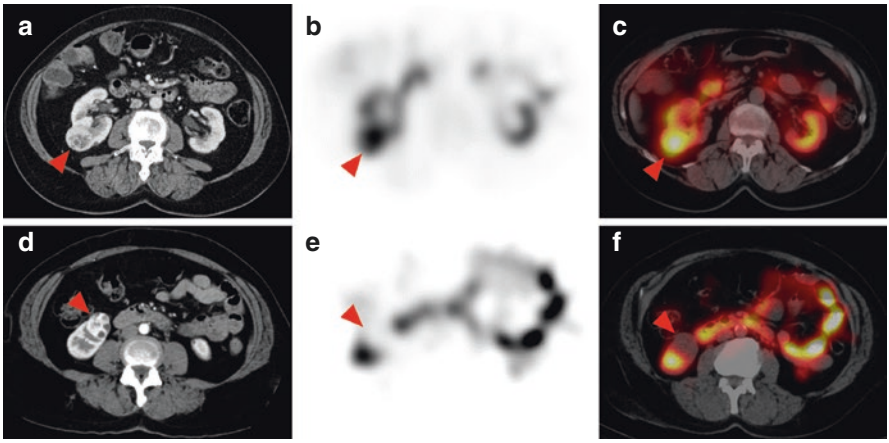

Fig. 4.7 Characterization of renal tumor histology using ^{99m}Tc-sestamibi SPECT/CT. (**a**) Axial, late arterial phase CT image from a patient with an indeterminate right renal mass (red arrowhead). (**b**) Axial ^{99m}Tc-sestamibi SPECT and (**c**) SPECT/CT images from the same patient show intense radiotracer uptake (red arrowheads), most compatible with a benign or indolent histology. This tumor was biopsied and found to be an oncocytic renal neoplasm. The patient is currently on active surveillance. (**d**) Axial, arterial phase CT from another patient with an indeterminate right renal mass (red arrowhead). (**e**) Axial ^{99m}Tc-sestamibi SPECT and (**f**) SPECT/CT images from the same patient demonstrate a lack of radiotracer uptake in the mass (red arrowheads), most compatible with an aggressive histology. This mass was resected and found to be a clear cell RCC

cation that has an intrinsic affinity for the high negative charge potential associated with mitochondrial membranes. Current common uses of ^{99m}Tc-sestamibi include myocardial perfusion imaging and localization of parathyroid adenomas. Interestingly, as early as 1996, Gormley and coworkers had the insight that mitochondria-rich oncocytomas might demonstrate differential uptake of ^{99m}Tc-sestamibi in comparison to other renal tumors [43]. Indeed, in a proof-of-principle study using non-tomographic imaging, the authors successfully identified an oncocytoma among several renal tumors [43]. Approximately 20 years later, Rowe et al. utilized the more detailed fusion of molecular and anatomic imaging available with SPECT/CT to further suggest the usefulness of ^{99m}Tc-sestamibi imaging in this context [44]. In their study, the authors successfully utilized ^{99m}Tc-sestamibi SPECT/CT to differentiate three oncocytomas apart from three aggressive RCCs. In a follow-up study that included 50 patients, Gorin and coworkers reported a sensitivity of 87.5% and a specificity of 95.2% for preoperatively identifying oncocytomas and closely related hybrid oncocytic/chromophobe tumors from other renal tumor types [45]. Additionally, initial results of a large diagnostic trial taking place in Sweden supported the high accuracy of this method for characterizing renal tumors as benign/indolent [46].

Beyond aiding in the characterization of clinically localized renal masses, molecular imaging also has potential to assist in staging patients with RCC. More specifically, ^{18}F-FDG PET/CT has proven to have a high degree of sensitivity for detecting sites of metastatic RCC [47]. It should be noted, however, that current

guidelines from the National Comprehensive Cancer Network do not endorse the routine use of this imaging modality due to a relative paucity of data to suggest that this expensive imaging modality is superior to contrast-enhanced CT [48]. Additional investigational PET agents that show promise for the detection of RCC metastases include ^{89}Zr-labeled bevacizumab (a monoclonal antibody against vascular endothelial growth factor [49]) and ^{18}F- and ^{68}Ga-labeled small molecular radiotracers targeted against prostate-specific membrane antigen [50, 51].

Conclusions

A number of modalities exist for imaging renal tumors including conventional anatomic methods (CT, MRI, and US) and molecular imaging approaches (PET and SPECT). Conventional imaging will most often be the means by which renal tumors are detected, either incidentally when a patient is being imaged for non-genitourinary complaints or when a patient is undergoing an evaluation for clinical signs and symptoms such as hematuria or flank pain. Conventional imaging provides important information regarding a detected renal mass including its solid or cystic nature, size, and stage in cases of malignancy. However, anatomic imaging often fails to differentiate benign from malignant clinically localized renal masses. For this reason, there is currently an increasing emphasis on using molecular imaging data to provide additional information on the underlying biology of renal masses. At the time of this writing, there is not a widely accepted molecular imaging test for characterizing renal tumors; however, several promising agents are in various stages of preclinical or early clinical development. In the future, it seems quite likely that molecular imaging will play an important role in the noninvasive risk stratification of clinically localized renal masses.

References

1. Gill IS, Aron M, Gervais DA, Jewett MA. Clinical practice. Small renal mass. N Engl J Med. 2010;362(7):624–34.
2. Hollingsworth JM, Miller DC, Daignault S, Hollenbeck BK. Rising incidence of small renal masses: a need to reassess treatment effect. J Natl Cancer Inst. 2006;98(18):1331–4.
3. Holger Moch PAH, Ulbright TM, Reuter VE. WHO classification of tumours of the urinary system and male genital organs: International Agency for Research on Cancer (IARC) 69372 Lyon Cedex 08, France; 2016.
4. Srigley JR, Delahunt B, Eble JN, Egevad L, Epstein JI, Grignon D, et al. The International Society of Urological Pathology (ISUP) Vancouver classification of renal neoplasia. Am J Surg Pathol. 2013;37(10):1469–89.
5. Johnson DC, Vukina J, Smith AB, Meyer AM, Wheeler SB, Kuo TM, et al. Preoperatively misclassified, surgically removed benign renal masses: a systematic review of surgical series and United States population level burden estimate. J Urol. 2015;193(1):30–5.
6. Gorin MA, Rowe SP, Allaf ME. Nuclear imaging of renal tumours: a step towards improved risk stratification. Nat Rev Urol. 2015;12(8):445–50.

7. Gorin MA, Rowe SP, Allaf ME. Noninvasive determination of renal tumor histology utilizing molecular imaging. Urol Oncol. 2016;34(12):525–8.
8. Pierorazio PM, Hyams ES, Tsai S, Feng Z, Trock BJ, Mullins JK, et al. Multiphasic enhancement patterns of small renal masses (</=4 cm) on preoperative computed tomography: utility for distinguishing subtypes of renal cell carcinoma, angiomyolipoma, and oncocytoma. Urology. 2013;81(6):1265–71.
9. Gakis G, Kramer U, Schilling D, Kruck S, Stenzl A, Schlemmer HP. Small renal oncocytomas: differentiation with multiphase CT. Eur J Radiol. 2011;80(2):274–8.
10. Gorin MA, Ball MW, Pierorazio PM, Tanagho YS, Bhayani SB, Kaouk JH, et al. Outcomes and predictors of clinical T1 to pathological T3a tumor up-staging after robotic partial nephrectomy: a multi-institutional analysis. J Urol. 2013;190(5):1907–11.
11. Bosniak MA. The current radiological approach to renal cysts. Radiology. 1986;158(1):1–10.
12. Jonisch AI, Rubinowitz AN, Mutalik PG, Israel GM. Can high-attenuation renal cysts be differentiated from renal cell carcinoma at unenhanced CT? Radiology. 2007;243(2):445–50.
13. Israel GM, Bosniak MA. Follow-up CT of moderately complex cystic lesions of the kidney (Bosniak category IIF). AJR Am J Roentgenol. 2003;181(3):627–33.
14. Smith AD, Remer EM, Cox KL, Lieber ML, Allen BC, Shah SN, et al. Bosniak category IIF and III cystic renal lesions: outcomes and associations. Radiology. 2012;262(1):152–60.
15. Gorin MA, Rowe SP, Allaf ME, Argani P. Angiomyolipoma with epithelial cysts: add one to the differential of cystic renal lesions. Int J Urol. 2015;22(11):1081–2.
16. Heilbrun ME, Remer EM, Casalino DD, Beland MD, Bishoff JT, Blaufox MD, et al. ACR Appropriateness Criteria indeterminate renal mass. J Am Coll Radiol. 2015;12(4):333–41.
17. Kang SK, Kim D, Chandarana H. Contemporary imaging of the renal mass. Curr Urol Rep. 2011;12(1):11–7.
18. Outwater EK, Bhatia M, Siegelman ES, Burke MA, Mitchell DG. Lipid in renal clear cell carcinoma: detection on opposed-phase gradient-echo MR images. Radiology. 1997;205(1):103–7.
19. Ramamurthy NK, Moosavi B, McInnes MD, Flood TA, Schieda N. Multiparametric MRI of solid renal masses: pearls and pitfalls. Clin Radiol. 2015;70(3):304–16.
20. Sasiwimonphan K, Takahashi N, Leibovich BC, Carter RE, Atwell TD, Kawashima A. Small (<4 cm) renal mass: differentiation of angiomyolipoma without visible fat from renal cell carcinoma utilizing MR imaging. Radiology. 2012;263(1):160–8.
21. Lassel EA, Rao R, Schwenke C, Schoenberg SO, Michaely HJ. Diffusion-weighted imaging of focal renal lesions: a meta-analysis. Eur Radiol. 2014;24(1):241–9.
22. Wang H, Cheng L, Zhang X, Wang D, Guo A, Gao Y, et al. Renal cell carcinoma: diffusion-weighted MR imaging for subtype differentiation at 3.0 T. Radiology. 2010;257(1):135–43.
23. Israel GM, Hindman N, Bosniak MA. Evaluation of cystic renal masses: comparison of CT and MR imaging by using the Bosniak classification system. Radiology. 2004;231(2):365–71.
24. Jamis-Dow CA, Choyke PL, Jennings SB, Linehan WM, Thakore KN, Walther MM. Small (< or = 3-cm) renal masses: detection with CT versus US and pathologic correlation. Radiology. 1996;198(3):785–8.
25. Pierorazio PM, Johnson MH, Ball MW, Gorin MA, Trock BJ, Chang P, et al. Five-year analysis of a multi-institutional prospective clinical trial of delayed intervention and surveillance for small renal masses: the DISSRM registry. Eur Urol. 2015;68(3):408–15.
26. Zirinsky K, Auh YH, Rubenstein WA, Williams JJ, Pasmantier MW, Kazam E. CT of the hyperdense renal cyst: sonographic correlation. AJR Am J Roentgenol. 1984;143(1):151–6.
27. Park BK, Kim B, Kim SH, Ko K, Lee HM, Choi HY. Assessment of cystic renal masses based on Bosniak classification: comparison of CT and contrast-enhanced US. Eur J Radiol. 2007;61(2):310–4.
28. Tamai H, Takiguchi Y, Oka M, Shingaki N, Enomoto S, Shiraki T, et al. Contrast-enhanced ultrasonography in the diagnosis of solid renal tumors. J Ultrasound Med. 2005;24(12):1635–40.
29. Raman SP, Chen Y, Schroeder JL, Huang P, Fishman EK. CT texture analysis of renal masses: pilot study using random forest classification for prediction of pathology. Acad Radiol. 2014;21(12):1587–96.

30. About Nuclear Medicine and Molecular Imaging [Internet]. Society of Nuclear Medicine and Molecular Imaging Website. Accessed 3 June 2017. Available from: http://www.snmmi.org/AboutSNMMI/Content.aspx?ItemNumber=6433.
31. Ozulker T, Ozulker F, Ozbek E, Ozpacaci T. A prospective diagnostic accuracy study of F-18 fluorodeoxyglucose-positron emission tomography/computed tomography in the evaluation of indeterminate renal masses. Nucl Med Commun. 2011;32(4):265–72.
32. Supuran CT. Carbonic anhydrases: novel therapeutic applications for inhibitors and activators. Nat Rev Drug Discov. 2008;7(2):168–81.
33. Grabmaier K, AdW MC, Verhaegh GW, Schalken JA, Oosterwijk E. Strict regulation of CAIX(G250/MN) by HIF-1alpha in clear cell renal cell carcinoma. Oncogene. 2004;23(33):5624–31.
34. Shuch B, Amin A, Armstrong AJ, Eble JN, Ficarra V, Lopez-Beltran A, et al. Understanding pathologic variants of renal cell carcinoma: distilling therapeutic opportunities from biologic complexity. Eur Urol. 2015;67(1):85–97.
35. Ivanov S, Liao SY, Ivanova A, Danilkovitch-Miagkova A, Tarasova N, Weirich G, et al. Expression of hypoxia-inducible cell-surface transmembrane carbonic anhydrases in human cancer. Am J Pathol. 2001;158(3):905–19.
36. Potter C, Harris AL. Hypoxia inducible carbonic anhydrase IX, marker of tumour hypoxia, survival pathway and therapy target. Cell Cycle. 2004;3(2):164–7.
37. Clare BW, Supuran CT. A perspective on quantitative structure-activity relationships and carbonic anhydrase inhibitors. Expert Opin Drug Metab Toxicol. 2006;2(1):113–37.
38. Divgi CR, Pandit-Taskar N, Jungbluth AA, Reuter VE, Gonen M, Ruan S, et al. Preoperative characterisation of clear-cell renal carcinoma using iodine-124-labelled antibody chimeric G250 (124I-cG250) and PET in patients with renal masses: a phase I trial. Lancet Oncol. 2007;8(4):304–10.
39. Divgi CR, Uzzo RG, Gatsonis C, Bartz R, Treutner S, Yu JQ, et al. Positron emission tomography/computed tomography identification of clear cell renal cell carcinoma: results from the REDECT trial. J Clin Oncol. 2013;31(2):187–94.
40. Yang X, Minn I, Rowe SP, Banerjee SR, Gorin MA, Brummet M, et al. Imaging of carbonic anhydrase IX with an 111In-labeled dual-motif inhibitor. Oncotarget. 2015;6(32):33733–42.
41. Minn I, Koo SM, Lee HS, Brummet M, Rowe SP, Gorin MA, et al. [64Cu]XYIMSR-06: a dual-motif CAIX ligand for PET imaging of clear cell renal cell carcinoma. Oncotarget. 2016;7(35):56471–9.
42. Ho CL, Chen S, Ho KM, Chan WK, Leung YL, Cheng KC, et al. Dual-tracer PET/CT in renal angiomyolipoma and subtypes of renal cell carcinoma. Clin Nucl Med. 2012;37(11):1075–82.
43. Gormley TS, Van Every MJ, Moreno AJ. Renal oncocytoma: preoperative diagnosis using technetium 99m sestamibi imaging. Urology. 1996;48(1):33–9.
44. Rowe SP, Gorin MA, Gordetsky J, Ball MW, Pierorazio PM, Higuchi T, et al. Initial experience using 99mTc-MIBI SPECT/CT for the differentiation of oncocytoma from renal cell carcinoma. Clin Nucl Med. 2015;40(4):309–13.
45. Gorin MA, Rowe SP, Baras AS, Solnes LB, Ball MW, Pierorazio PM, et al. Prospective evaluation of (99m)Tc-sestamibi SPECT/CT for the diagnosis of renal oncocytomas and hybrid oncocytic/chromophobe tumors. Eur Urol. 2016;69(3):413–6.
46. Tzortzakakis AGO, Karlsson M, Ekstrom-Ehn L, Ghaffarpour R, Axelsson R. Visual evaluation and differentiation of renal oncocytomas from renal cell carcinomas by means of 99mTc-Sestamibi SPECT/CT. EJNMMI Res. 2017;7:29.
47. Wang HY, Ding HJ, Chen JH, Chao CH, Lu YY, Lin WY, et al. Meta-analysis of the diagnostic performance of [18F]FDG-PET and PET/CT in renal cell carcinoma. Cancer Imaging. 2012;12:464–74.
48. Motzer RJ, Jonasch E, Agarwal N, Bhayani S, Bro WP, Chang SS, et al. Kidney Cancer, version 2.2017, NCCN clinical practice guidelines in oncology. J Natl Compr Cancer Netw. 2017;15(6):804–34.

49. Oosting SF, Brouwers AH, van Es SC, Nagengast WB, Oude Munnink TH, Lub-de Hooge MN, et al. 89Zr-bevacizumab PET visualizes heterogeneous tracer accumulation in tumor lesions of renal cell carcinoma patients and differential effects of antiangiogenic treatment. J Nucl Med. 2015;56(1):63–9.
50. Rowe SP, Gorin MA, Hammers HJ, Som Javadi M, Hawasli H, Szabo Z, et al. Imaging of metastatic clear cell renal cell carcinoma with PSMA-targeted (18)F-DCFPyL PET/CT. Ann Nucl Med. 2015;29(10):877–82.
51. Sawicki LM, Buchbender C, Boos J, Giessing M, Ermert J, Antke C, et al. Diagnostic potential of PET/CT using a 68Ga-labelled prostate-specific membrane antigen ligand in whole-body staging of renal cell carcinoma: initial experience. Eur J Nucl Med Mol Imaging. 2017;44(1):102–7.